NONDESTRUCTIVE ASSESSMENT OF AEROSPACE COMPONENTS BY MEANS OF PULSED THERMOGRAPHY

C. Ibarra-Castanedo, C. Mohr, X. P. Maldague and A. Bendada
Computer Vision and Systems Laboratory
Department of Electrical and Computer Engineering
Laval University, Quebec City, Canada. G1K 7P4
IbarraC@gel.ulaval.ca

P. Servais
Belgian Air Force
Competence Center Flying Material
Center Flying Material, Non Destructive Testing Squadron
1130 Brussel, Belgium

ABSTRACT

Infrared (IR) thermography is a nondestructive, non-contact and non-intrusive technique that allows the fast inspection of large and complex structures with limited accessibility. Pulsed thermography is particularly interesting for the inspection of aerospace materials such as composites given that, after submitting the specimen surface to a thermal front, the most common types of subsurface discontinuities (*e.g.* porosity, delaminations, disbonds, fiber breakage and inclusions) can be detected with an IR camera as regions showing abnormal temperature patterns. We present first the case of an aircraft door with water ingress and surface repairs on its honey comb structure. We also highlight the advantages and limitations of thermography for the inspection of aircraft composite parts, such as edge flaps, rotor blades and speed breaks. Finally, we expose some results from a Kevlar® non-planar specimen with Teflon® inclusions at different depths and locations.

Keywords: Infrared thermography, nondestructive evaluation, composites, non-planar inspection.

INTRODUCTION

The role of aircraft inspection and maintenance has progressively increased since the 1980s when it became evident that aircrafts were exceeding their original design lives and that early detection and repair was critical to avoid catastrophic events [1, 2]. Composite materials are probably the material most widely used in the aerospace industry nowadays. Fiber reinforced plastics are a common type that are made of carbon (CFRP), glass (GFRP), Kevlar®, Nomex® or other fibers embedded in an epoxy matrix to form a ply that can be combined with other plies and shaped to form different structures. Each ply is usually rotated by a determined angle with respect to adjacent plies in order to improve strength. Examples of application include: speed brakes and rotor blades. Sandwiched structures are another important category of composites. They consists of two metallic, plastic or composite skins having great mechanical strength separated by a core spacer made of a low-density material such as honeycomb or foam, providing better distribution of loading than a simple laminate [4]. Many aircraft parts are now produced using sandwiched structures: ailerons, flaps, keels, rudders, etc. [5].

There are several ways in which the integrity of composite components can be impaired. During the fabrication stages, subsurface flaws such as voids, delaminations, inclusions, porosity and regions having unbalanced fiber content, may result from inadequate production procedures. Subsequent machining, *e.g.* drilling or cutting, may produce cracks and delaminations if improperly executed. Aerospace parts can be affected during normal operation as well. For instance, impact of hard bodies, *e.g.* birds or artillery, may damage (fiber breakage) the fuselage and other parts surfaces, or atmosphere water can penetrate the core due to possible imperfections in junctions [3, 4].

Visual inspection and sonic tap have been widely used for inspection. However, the industry is being gradually moving towards qualitative and quantitative techniques relying to a lesser extends in the skills and training of an operator. There are several techniques in use at present [4, 6]: optical testing (shearography, holography), radiographic inspection (neutron radiography, X-rays), eddy current, thermal methods (thermography) and ultrasounds, with the later being perhaps the most commonly used inspection technique for aerospace components. In conventional ultrasonic testing, the transducer must be maintained normal to the part during the acquisition [6], which is relatively easy to perform on small flat parts but it is more complicated during inspection of non-planar and large surfaces. Further complications are related to the high degree of automation and advanced data processing that are required [2]. Infrared thermography is gaining popularity thanks to its rapidity and easiness of inspection. For instance, trapped water at cruising flight height becomes frozen and remains cold long time (2 to 3 hours) after landing, which allows to *passively*, *i.e.* without using any external source of energy, detecting water. In contrast, quantitative evaluation is difficult to perform on such a scheme. Ultrasounds on the contrary would have no problem on assessing water content by determining the height of a water column in a cell for example [5]. However, it could take long time to identify the regions with water ingress in a point-to-point technique. An interesting approach is to combine both techniques: thermography can be used for the initial detection and ultrasounds for subsequent characterization [2].

On the other hand, *active* thermography can be considered as a completely autonomous technique, competing in some cases with ultrasounds in terms of accuracy of detection [6]. Furthermore, in some cases active thermography might be the most suitable technique to perform the inspection, *e.g.* when only one side of the specimen is available and for detecting corrosion around rivets [7].

In this paper, we present the basic configuration for *pulsed* thermography data acquisition; we review three advanced signal processing techniques and illustrate their applications through some examples.

PULSED THERMOGRAPHY

Data acquisition

Active infrared thermography is a nondestructive evaluation (NDE) technique allowing fast inspection of large surfaces, in which the inspected specimen is thermally stimulated with an external energy source. In pulsed thermography, a heat pulse is used as an energy source. Data acquisition and processing is carried out as depicted in Figure 1 and can be summarized as follows.
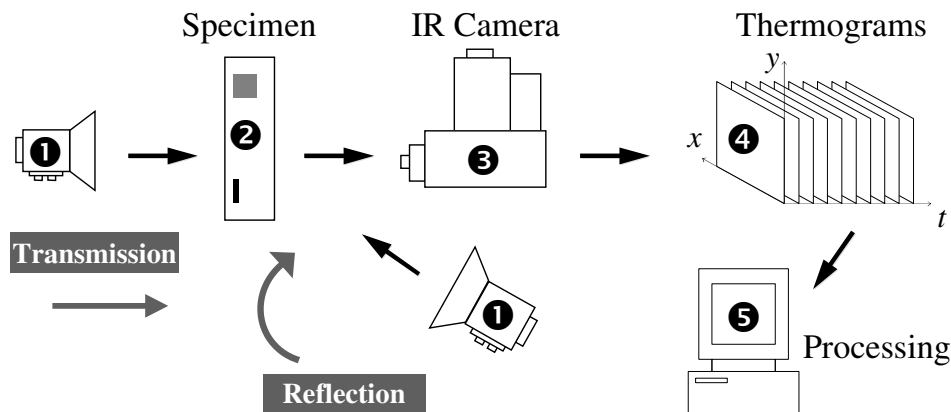

Figure 1 − Data acquisition and processing in active thermography.

First, the specimen surface is stimulated with a thermal pulse ❶ in either transmission or reflection mode depending on the application. Heating (or cooling) may be delivered in transitory regime (*e.g.* as a pulse of a few milliseconds or as a step of several seconds). A steady state configuration is also possible, *e.g.* as periodic waves for several seconds, which is known as lock-in thermography or modulated thermography [8]. Defective zones will appear at higher or lower temperature with respect to non-defective zones on the surface, depending on the thermal properties of both, the material and the defect ❷. The thermal signatures are recorded using an infrared camera ❸. A thermal map of the surface or a *thermogram* is recorded at regular time intervals. A 3D matrix is formed ❹, where x and y coordinates are the horizontal and vertical pixel positions respectively, and the z coordinate corresponds to time. The thermogram matrix is ready to be processed ❺.

Processing techniques

There are a great variety of processing techniques that have being used to enhance the subtle IR signatures. Space being limited, it is not possible to discuss in details all of them. We selected three techniques that have shown very promising results for aerospace applications. Although only a brief discussion is provided; interested readers may consult the references provided below.

Differential absolute contrast method

Various thermal contrast definitions exist [7, p. 198], but they all share the need to specify a sound area S_a, *i.e.* a non-defective region within the field of view. For instance *absolute* thermal contrast $\Delta T(t)$ is defined as [7]:

$$\Delta T(t) = T_d(t) - T_{S_a}(t) \tag{1}$$

with $T(t)$ being the temperature at time t, $T_d(t)$ the temperature of a pixel p (defective or not) or the average value of a group of pixels, and $T_{Sa}(t)$ the temperature at time t for the S_a. No defect can be detected at a particular t if $\Delta T(t)=0$.

The main drawback of classical thermal contrast is establishing S_a, especially if automated analysis is needed. Even when S_a definition is straightforward, considerable variations on the results are observed when changing the location of S_a as is well-known [9].

The differential absolute contrast (DAC) method [10] is based on the 1D solution of the Fourier diffusion equation for a Dirac pulse uniformly applied to the surface ($z=0$) of a semi-infinite body, which may be written as follows [11]:

$$T(t) = \frac{Q}{e\sqrt{\pi \cdot t}} \tag{2}$$

where $T(t)$ is the temperature evolution, Q is the injected energy at the surface, $e=(k\rho c_P)^{1/2}$ is the thermal effusivity of the sample.

In the DAC method, instead of looking for a non-defective area, the S_a temperature at time t is computed locally at p assuming that on the first few images (at time t' in particular, see below) local point p behaves as a S_a [10]. The first step is to define t' as a given time value between the instant when the pulse has been launched t_0, and the precise moment when the first defective spot appears on the thermogram sequence, *i.e.* when there is enough contrast for the defect to be detected, t_1. At t', there is no indication of the existence of a defective zone yet, therefore the local temperature for a S_a is exactly the same as for a defective area [12]:

$$T_{S_a}(t') = T(t') = \frac{Q}{e\sqrt{\pi t'}} \quad \Rightarrow \quad \frac{Q}{e} = \sqrt{\pi t'} \cdot T(t') \tag{3}$$

From this result, T_{Sa} can be computed for every pixel at time t. Substituting Eq. (3) into the absolute contrast definition, $i.e.$ Eq. (1), it follows that [12]:

$$\Delta T_{dac} = T(t) - \sqrt{\frac{t'}{t}} \cdot T(t')$$

(4)

Actual measurements diverge from the solution provided by Eq. (4) as time elapses and also as plate thickness enlarges with respect to the non-semi-infinite case. Nevertheless, it has proven to be very efficient in reducing artifacts from non-uniform heating and surface geometry [13], and to provide a good approximation even for the case of anisotropic materials [13, 14]. Originally, proper selection of t' required an iterative graphical procedure, for which a graphical user interface was developed [15]. An automated algorithm is now available [16].

Pulsed phase thermography

Pulsed phase thermography (PPT) [17] is another interesting technique, in which data is transformed from the time domain to the frequency spectra using the one-dimensional discrete Fourier transform (DFT) [17]:

$$F_n = \Delta t \sum_{k=0}^{N-1} T(k\Delta t) \exp^{(-j2\pi nk/N)} = \mathrm{Re}_n + \mathrm{Im}_n$$

(5)

$$A_n = \sqrt{\mathrm{Re}_n^2 + \mathrm{Im}_n^2} \quad and \quad \phi_n = \tan^{-1}\left(\frac{\mathrm{Im}_n}{\mathrm{Re}_n}\right)$$

(6)

where n designates the frequency increments ($n=0,1,\ldots N$), Δt is the sampling interval and Re and Im are respectively the real and the imaginary parts of the transform.

The fast Fourier transform (FFT) algorithm, available in MATLAB® `fft(...)`, is very convenient for NDE applications. Real and imaginary parts of Eq. (5) can be used to calculate the amplitude and the phase delay (or simply the phase) of the transform as in Eq. (6).

Phase ϕ is of particular interest in NDE given that it is less affected than raw thermal data by environmental reflections, emissivity variations, non-uniform heating, surface geometry and orientation. These phase characteristics are very attractive not only for qualitative inspections but also for quantitative characterization of materials [18].

Thermographic Signal Reconstruction

Thermographic signal reconstruction (TSR) [19] is an attractive technique that allows increasing spatial and temporal resolution of a sequence, reducing at the same time the amount of data to be manipulated. TSR is based on the assumption that, temperature profiles for non-defective pixels should follow the decay curve given by the

one-dimensional solution of the Fourier Equation, *i.e.* Eq. (2), which may be rewritten in the logarithmic form as:

$$\ln(\Delta T) = \ln\left(\frac{Q}{e}\right) - \frac{1}{2}\ln(\pi t) \tag{7}$$

Next, an *n*-degree polynomial is fitted for each pixel *p* within the field of view [19]:

$$\ln(\Delta T) = a_0 + a_1 \ln(t) + a_2 \ln^2(t) + \ldots + a_n \ln^n(t) \tag{8}$$

Typically, *n* is set to 4 or 5 to avoid "ringing" and to insure a good correspondence between data and fitted values. MATLAB® provides a direct polynomial fitting function `polyfit(...)`. Synthetic data processing brings interesting advantages such as: significant noise reduction, possibility for analytical computations, considerably less storage required since the whole data set is reduced to *n*+1 images (one per coefficient), and calculation of first and second time derivatives from the synthetic coefficients is straightforward.

Next section presents three different cases in which these techniques were applied. First, an aircraft door with water ingress and surface repairs on its honeycomb structure is tested. Second, we consider a calibration plate that allows assessing the viability of thermography to inspect aircraft composite parts (leading edge flaps, rotor blades and speed breaks). Finally, we expose some results from a calibration Kevlar® non-planar specimen with Teflon® inserts.

EXPERIMENTAL RESULTS

Honeycomb aircraft door

Figure 2 shows a GFRP door with a honeycomb core developed for Airbus by SABCA Limburg N. V. (Société anonime belge de constructions aéronautiques).
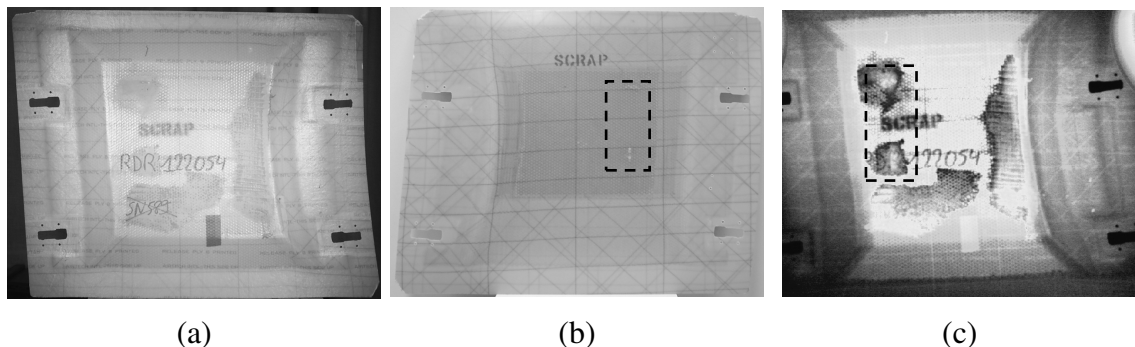

(a)   (b)   (c)

Figure 2 – Photographs of the airbus door: (a) front view, and (b) rear view; and (c) whole surface thermogram at *t*=1.2 s after pulse heating in reflection.

Photographs displaying the front and rear views are seen in Figure 2a and b, respectively, while a thermogram 1.2 s after pulse-heating the specimen front side is presented in Figure 2c. Both the front view photograph and the thermogram (Figure 2a and c, respectively) clearly exhibit four distinctive repair zones at the surface. The rear view photograph (Figure 2b) on the contrary shows no repairs but two water ingress spots. Figure 3a displays a zoomed portion (black dotted rectangle in Figure 2b) of the door. It is difficult to detect any water from the raw thermogram in Figure 2c. However, it is possible to process the thermal sequence using the techniques described above.
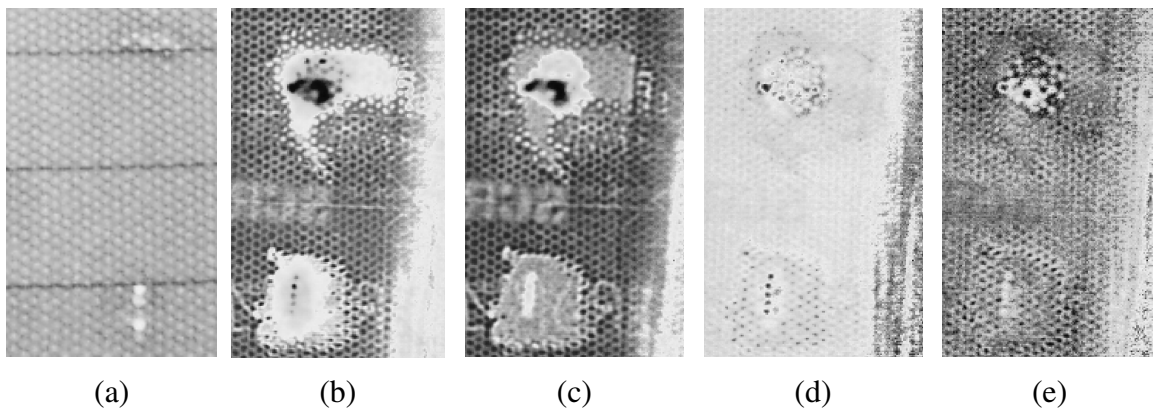

| (a) | (b) | (c) | (d) | (e) |

Figure 3 − (a) Photograph showing the zoomed portion in the back side of the panel as indicated in Figure 1b. TSR results from a 9th degree polynomial: first derivatives at $t=$ (b) 1.2 and (c) 2.16 s; and second derivatives for a at $t=$ (d) 2.83 and (e) 3.41 s.

For example, Figure 3b to e correspond to first and second time derivatives obtained by TSR at different times as indicated in the figure legend. These images were selected in order to enhance the contrast of the different honeycomb cells with water ingress and they were inverted with respect to the y-axis to be compared with the photograph in Figure 3a (notice that letters "SCR" in Figure 3b and c are actually reversed). The specimen however, was tested in reflection mode from the front side as seen in Figure 2c. The honeycomb structure is clearly visible in all the images although contrast is better in first derivatives (Figure 3b and c). Second derivatives exhibit cells containing water with improved contrast for the bottom (Figure 3d) and the top (Figure 3e) spots.

Calibration plate for aircraft composite parts

Composites are widely used in aeronautical applications. For instance, leading edge flaps of Belgian F-16 aircraft, and main and tail rotor blades of Belgian Augusta helicopter, which are exclusively built in composite [20], and Alphajet speed breaks. Tap testing is still a standard technique to verify the integrity of these parts since radiographic techniques are not suitable for the inspection of delaminations (an important type of defect in these parts) and ultrasonic tests are impractical due to lengthy point-to-point procedures.

Calibration plates such as the one appearing in Figure 4a were used in order to test the suitability of infrared thermography for the control of these parts. The plate in Figure 4a was produced by Dassault for the Belgian Airforce and it consists of 12 CFRP plies (0–45–90°) containing 10 Teflon® inclusions of two diameters (5 and 10 mm), which simulate delaminations at different depths and locations as depicted. The plate was tested by pulsed thermography using a 5 ms heat pulse and a frame rate of 157 Hz and then processed by PPT.
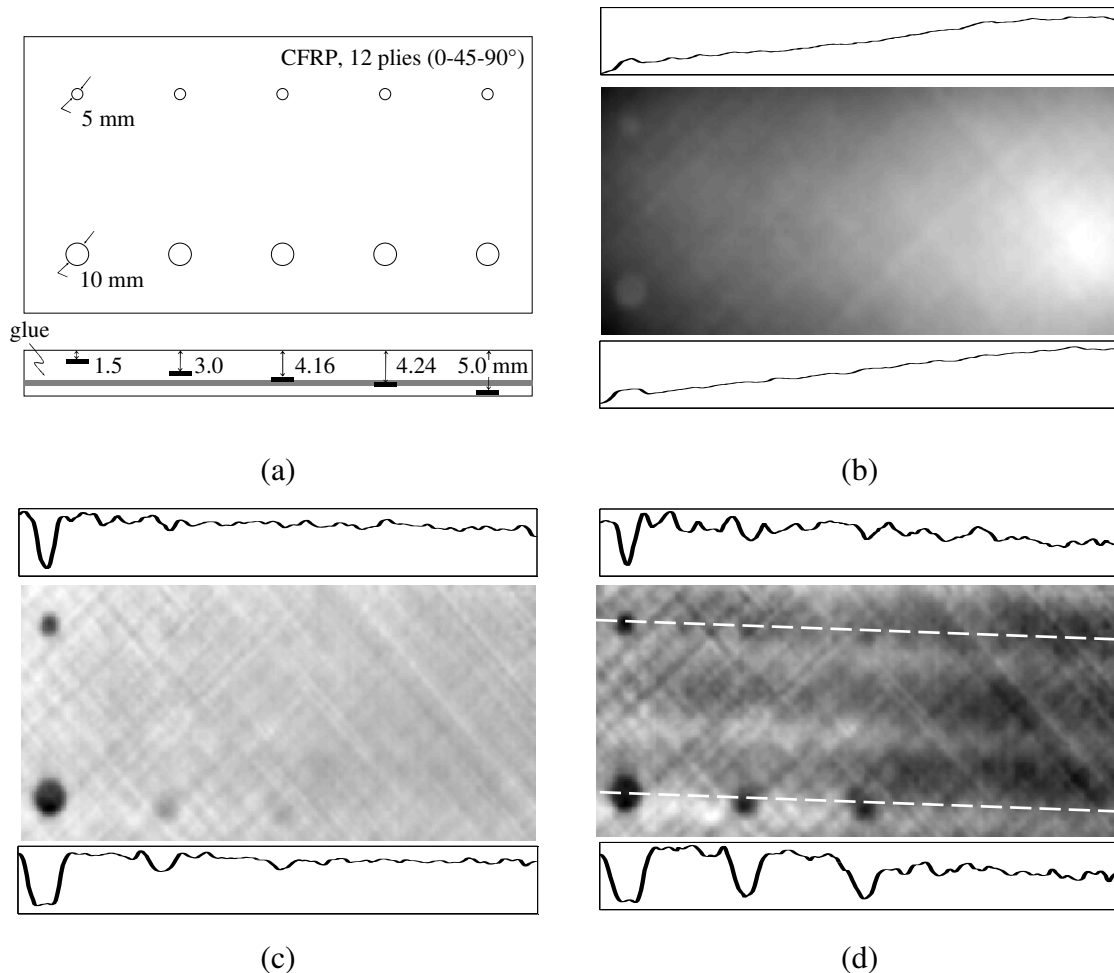

(a)

(b)

(c)

(d)

Figure 4 – CFRP calibration plate: (a) geometry, (b) thermogram at t=754 ms showing the two shallowest defects, and phasegrams at f= (c) 0.316, and (e) 0.158 Hz.

Figure 4b displays a raw thermogram 754 ms after the heat pulse. The quasi-horizontal 1D spatial profiles below the thermogram (following the line of defects as depicted in Figure 4d) testifies of a strong non-uniform heating at the surface. This is a very common problem in pulsed thermography, which in this case contributes to 'hide' deep defects allowing the detection of only the shallowest ones. Fortunately, it is possible to minimize the effect of heating non-uniformities with processing techniques such as PPT. Figure 4c and b show phasegrams at 0.316 and 0.158 Hz, respectively.

Low frequencies are associated to deep features and high frequencies to shallow defects. Hence, for the three detectable 10 mm defects (bottom line of defects), the 0.158 Hz phasegram (Figure 4d) provides better contrast than the 0.316 Hz phasegram (Figure 4c). Fiber content and orientation is also clearly visible in both phasegrams. For the case of the 5 mm diameter defects (top line), although there is an indication of the presence the three shallowest defects (depths=1.5, 3.0 and 4.16 mm), only the 1.5 mm depth defect is detected with good contrast (*i.e.* considerably higher than noise) as seen from the spatial profiles. This observation confirms an old thumb rule in active thermography, which states that the defect size (the diameter D for circular defects) should be at least twice its depth z, *i.e.* $D / z \geq 2$, to provide good contrast. Although larger defects (D=10 mm) at z=4.24 and 5 mm comply with this empirical rule, the glue layer between plates (see cross section in Figure 4a) acts as an additional heat resistance preventing the detection of these two defects.

Kevlar® non-planar specimen

Many aerospace parts contain non-planar surfaces that are difficult to inspect with traditional NDE techniques. Infrared thermography is an interesting alternative for this matter as illustrated with the Kevlar® panel shown in Figure 5a. A total of 16 Teflon® inserts are distributed at different locations as indicated.
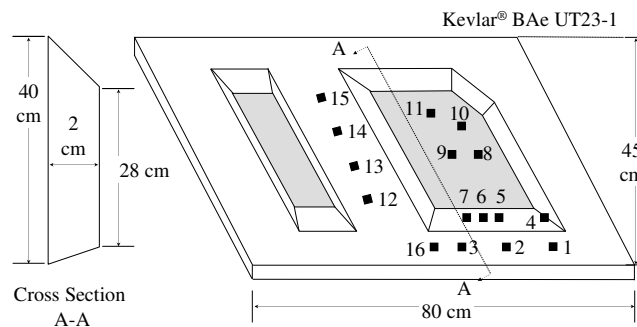
(a)
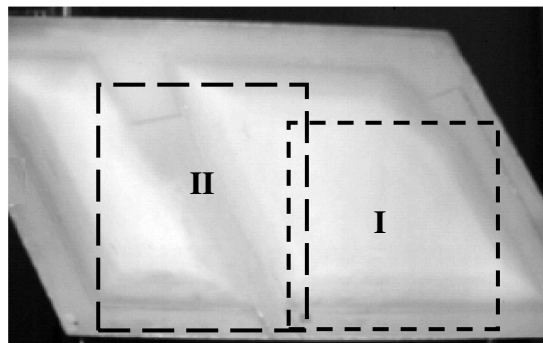
(b)

Figure 5 – Kevlar® specimen: (a) geometry, and (b) early recorded thermogram (immediately after the heat impulse) of the entire panel.

The specimen was inspected in two parts: regions I and II, delimited in Figure 5b. Raw thermograms together with results from DAC and TSR are presented in Figure 6 for region I (top) and region II (bottom).
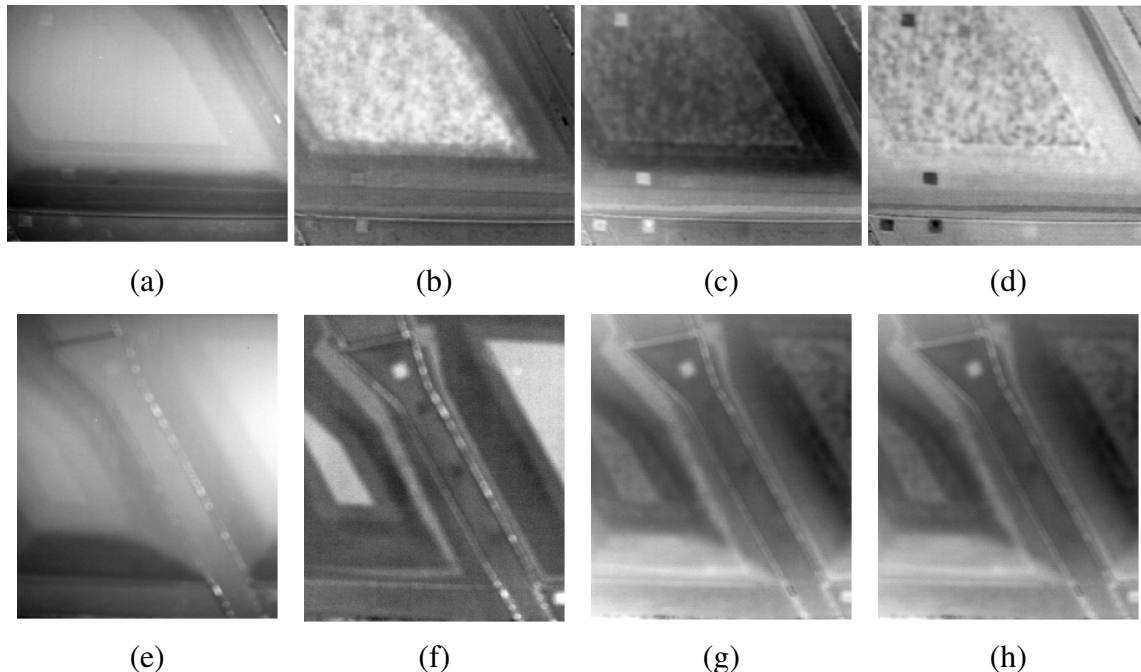

<div align="center">(a)   (b)   (c)   (d)</div>

<div align="center">(e)   (f)   (g)   (h)</div>

Figure 6 − Results for region I: (a) raw temperature at t=355 ms, (b) DAC at t=532 ms; (c) first and (d) second derivatives at t=177 ms. Region II: (e) raw temperature at t=355ms; (f) DAC at t=355 ms; (c) first and (d) second time derivatives at t=177 ms.

The raw thermogram 355 ms after the flash (Figure 6a) reveals the presence of 5 of 10 defects present in region I (Figure 5a), *i.e.* defects 3, 6, 7, 11 and 16. DAC processing (Figure 6b) allows detecting defect 10 as well. Defect 2 is visible in the first (Figure 6c) and second (Figure 6d) derivative images at 177 ms with increased contrast (although defect 6 is not clearly seen in Figure 6d). For region II, DAC result (Figure 6c) provides the best overall contrast, revealing the presence of the four defects. Although the non-planar shape of the surface is still seen, processing results with DAC and TSR greatly improves the defect contrast.

CONCLUSIONS

Pulsed thermography is an interesting NDE technique allowing the fast inspection of large surfaces. Its use is limited to relatively shallow defects (a few millimeters in depth), for which it size to depth ratio is at least equal to two ($D / z \geq 2$). This type of defects can be found in many practical applications, like the detection of water ingress in honeycomb structures and delaminations in composite parts. Non-planar inspection is also possible thanks to advanced processing techniques that minimize the effect of non-uniform heating, variability in surface emissivity, background reflections and surface geometry.

REFERENCES

1. Ducar R.J. "Pulsed thermographic inspection and application in commercial aircraft repair," Dennis H. LeMieux, J.R. Snell (eds.), *Proc. SPIE, Thermosense XXI*, **3700**:77-83, 1999.

2. Achenbach J.D. "Quantitative nondestructive evaluation," *Int. J. Solids Struct.*, **37**:13-27, 2000.

3. NDT Handbook on Infrared technology, ASNT Handbook Series, X. Maldague technical, P.O. Moore (eds.), ASNT Press (American Society for NonDestructive Testing) Press, 718 p., 2001.

4. Marinetti S., Muscio A., Bison P.G. and Grinzato E. "Modeling of thermal non-destructive evaluation techniques for composite materials," Ralph B. Dinwiddie, Dennis H. LeMieux (eds.), *Proc. SPIE, Thermosense XXII*, **4020**:164-173, 2000.

5. Vavilov V., Klimov A., Nesteruk D. and Shiryaev V. "Detecting water in aviation honeycomb structures by using transient IR thermographic NDT," Elliot Cramer, Xavier P. Maldague (eds.), *Proc. SPIE, Thermosense XXV*, **5073**:345-355, 2003.

6. Taylor J.O. and Dupont H.M. "Inspection of metallic thermal protection systems for the X-33 launch vehicle using pulsed infrared thermography," J. R. Snell, R. N. Wurzbach (eds.), *Proc. SPIE, Thermosense XX*, **3361**:301-310, 1998.

7. Maldague X.P.V., *Theory and Practice of Infrared Technology for NonDestructive Testing*, John Wiley-Interscience, 684 p., 2001.

8. Busse G., Wu D. and Karpen W. "Thermal Wave Imaging with Phase Sensitive Modulated Thermography," *J. Appl. Phys.*, 71(8): 3962-3965, 1992.

9. Martin R.E., Gyekenyesi A.L., Shepard S.M., "Interpreting the Results of Pulsed Thermography Data," Materials Evaluation, **61**(5):611-616, 2003.

10. Pilla M., Klein M., Maldague X. and Salerno A., "New Absolute Contrast for Pulsed Thermography," QIRT 2002, D. Balageas, G. Busse, G. Carlomagno (eds.), *Proc. of QIRT*, pp. 53-58, 2002.

11. Carslaw H.S. and Jaeger J.C., *Conduction of Heat in Solids*, 2nd edition, Clarendon Press, Oxford.

12. Pilla M. "A Novel Contrast Method for Pulse Thermography Data", *Ph.D. Thesis*, Politecnico di Milano, 2002.

13. Ibarra-Castanedo C., Bendada A. and Maldague X. "Image and signal processing techniques in pulsed thermography," *GESTS Int'l Trans. Computer Science and Engr.,* **22**(1): 89-100, November 2005.

14. Benitez H., Ibarra-Castanedo C., Bendada A., Maldague X. and Loaiza H. "Modified differential absolute contrast using thermal quadrupoles for the nondestructive testing of finite thickness specimens by infrared thermography," *CCECE 2006 - Canadian Conference on Electrical and Computer Engineering,* Papier No. **398**, Ottawa (Ontario) Canada, 7-10 mai, 2006.

15. Klein, M., Pilla M. and Maldague X. "IR_View: A graphical user interface to process infrared images with MATLAB," application and documentation available online [http://irview.m-klein.com].

16. González D.A., Ibarra-Castanedo C., Pilla M., Klein M., López-Higuera J.M. and Maldague X., "Automatic Interpolated Differentiated Absolute Contrast Algorithm for the Analysis of Pulsed Thermographic Sequence," *Proc. 7th Conference on Quantitative InfraRed Thermography (QIRT)*, Rhode Saint Genèse, Belgium, July 5-8, 2004, H.16.1-H.16.6.

17. Maldague X. and Marinetti S., "Pulse Phase Infrared Thermography," *J. Appl. Phys.*, **79**:2694-2698, 1996.

18. Ibarra-Castanedo C. "Quantitative subsurface defect evaluation by pulsed phase thermography: depth retrieval with the phase," *Ph. D. thesis*, Laval University, 2005. [accessible online: http://www.theses.ulaval.ca/2005/23016/23016.pdf].

19. Shepard S.M. "Advances in Pulsed Thermography", Andres E. Rozlosnik, Ralph B. Dinwiddie (eds.), *Proc. SPIE, Thermosense XXIII*, **4360**:511-515, 2001.

20. Servais P. and Gerlach N. "Development of a NDT method using thermography for composite material inspection on aircraft using military thermal imager," X. Maldague (ed.), *Proc. Vth International Workshop, Advance in signal Processing for Non Destructive Evaluation of Materials*, Quebec City (Canada), 2-4 August, pp. 197-202, 2005.